Journal of Alloys and Compounds 508 (2010) 419–425

Contents lists available at ScienceDirect

Journal of Alloys and Compounds

journal homepage: www.elsevier.com/locate/jallcom

Investigations of DC-magnetization behavior of nanocrystalline ZnO:Ni

Vidhi Goyal[a], Kanwal Preet Bhatti[b,*], Sujeet Chaudhary[a]

[a] Department of Physics, Indian Institute of Technology Delhi, New Delhi 110016, India
[b] Department of Physics, Guru Nanak Dev University, Amritsar 143005, India

ARTICLE INFO

Article history:
Received 1 June 2010
Received in revised form 13 August 2010
Accepted 24 August 2010

PACS:
75.50.Pp
75.50.Dd
75.60.Ej

Keywords:
Magnetically ordered materials
Oxide materials
Magnetic measurements

ABSTRACT

Ferromagnetic character observed in chemically synthesized nanocrystalline ZnO:Ni (upto 10 at% Ni) powder samples has been tracked vis-à-vis the processing conditions. The DC-magnetization behavior is found to be strongly dependent upon the employed sample processing conditions. While the as-calcined samples are strongly ferromagnetic due to the presence of nickel clusters; sintering of the samples to higher temperature in air ambient oxidizes Ni clusters and the magnetic behavior of the samples undergo significant changes. The samples are no longer completely ferromagnetic and are a mixture of ferromagnetic, antiferromagnetic, paramagnetic and diamagnetic fractions, depending upon the temperature dependent solubility limit of Ni in ZnO. This work further clearly suggests that the weak room temperature ferromagnetism observed in the ZnO:Ni samples (upto 10 at% Ni), sintered in air at 900 °C/12 h, is an intrinsic effect.

1. Introduction

Ferromagnetic semiconductors (FMSs) are one of the promising materials in the emerging field of spintronics. For realizing practical devices, a key requirement is that the host material should be ferromagnetic at or above room temperature. Due to the outstanding optical and electrical properties, considerable attention has been focused on ZnO-based FMSs in the past few years. Magnetic characteristics and possible mechanisms have been studied theoretically [1,2] and experimentally in ZnO doped with transition metals [3–12]. Ferromagnetism with a Curie temperature (T_C) higher than room temperature has been reported in many cases in Co doped ZnO [3,4]. In the case of Ni doped ZnO, relatively fewer studies have been reported since its preparation is particularly challenging due to the large driving force for phase segregation into NiO and ZnO. In the case of Ni doped ZnO, thin films prepared by spin coating [5], direct current magnetron cosputtering [6,7], pulsed laser deposition [8–10], sol–gel [11], rf magnetron sputtering [13,14] and electrochemical means [15] have been studied. In some cases, nickel doped ZnO nanocrystals [16] and thin films [13] are found to be paramagnetic. However, in other cases, nanocrystalline powder samples [17–19] and nanorods [20] are reported to be ferromagnetic or even superparamagnetic [21]. Large variations in magnetic properties for Ni doped ZnO indicate that ferromagnetism in this system strongly depends on the methods and conditions used in their preparation. Moreover, even the conclusion of intrinsic ferromagnetism remains controversial. In some cases, the observed room temperature ferromagnetism (RTFM) was claimed to be carrier mediated [19,23] or occurring due to defects [22] or oxygen vacancies [24–26]. Still in a few other cases, Ni clusters were responsible for observed RTFM [27–29]. It is also reported that homogeneous incorporation of Ni in ZnO results in paramagnetic samples, whereas the imperfectly doped samples lead to ferromagnetism [30]. In case of ZnO samples codoped with Li and Ni, it is observed that the insulating films are superparamagnetic, whereas the n and p type films exhibit RTFM [25]. Therefore, detailed study of the influence of doping concentration on ferromagnetism is particularly necessary and effective for understanding the intrinsic origin of ferromagnetism.

In the present work, we report the results of detailed investigation and the possible origin of the observed magnetic behavior in chemically synthesized nanocrystalline $Zn_{1-x}Ni_xO$ powder samples. The results of the effect of processing parameters on the magnetization (M), structural and phase purity of the nickel substituted ZnO nanocrystalline powder samples are presented in this paper.

2. Experimental

The chemical method for the synthesis of oxide particles was chosen as it results in better homogeneity and the obtained powders have smaller grain size as com-

* Corresponding author. Fax: +91 183 2258819.
E-mail address: kanwalbhatti@gmail.com (K.P. Bhatti).

0925-8388/$ – see front matter © 2010 Elsevier B.V. All rights reserved.
doi:10.1016/j.jallcom.2010.08.078

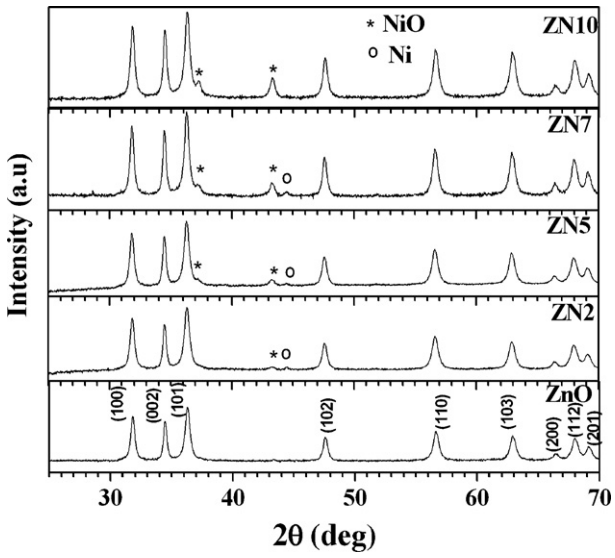

Fig. 1. Semilog XRD plots of as-calcined ZN0, ZN2, ZN5, ZN7 and ZN10 samples. The peaks arising due to NiO and Ni phases are indicated by symbols '*' and 'o', respectively.

pared to the conventional solid-state reaction method. The chemical route is a simple and cost effective route for the synthesis of various materials. Additionally, it is a low temperature process as compared to solid-state reaction method. Since the powders of the constituents are mixed in water or an organic solvent, the constituents mix at the molecular level and result in better homogeneity. In the present case nanocrystalline powders of ZnO:Ni, with 0, 2, 5, 7 and 10 at% Ni (named as ZN0, ZN2, ZN5, ZN7 and ZN10), were synthesized by chemical method using zinc acetate dihydrate, ($Zn(CH_3COO)_2{\cdot}2H_2O$), (purity 99.9%), nickel acetate tetrahydrate, ($Ni(CH_3COO)_2{\cdot}4H_2O$), (purity 99.9%) and polyvinylpyrrolidone (PVP) as precursors. For preparing the samples, the constituents in the desired proportion, were dissolved in DI water and stirred for 1 h. The solution was then dried at 90 °C on a hot plate. The dried mass so formed was calcined at 500 °C for 1 h. The calcined material was ground to fine powder and then pelletized. The role of the PVP is twofold: (a) it controls the growth of the particles by forming passivation layers around the ZnO core via coordination bond formation between the nitrogen atom of the PVP and Zn^{2+} ion, and/or (b) it prevents agglomeration by steric effect due to the repulsive force acting among the polyvinyl groups (tail part). Therefore, the PVP encapsulation creates a restricted environment around the ZnO nanocrystals.

After sintering at each temperature, the pellets were characterized for phase and structural analysis using x-ray diffractometer (Philips, Model X'Pert PRO) in Bragg Brentano geometry, and for magnetic properties using vibrating sample magnetometer (EG&G-PAR, Model 155). The high temperature magnetization measurements were carried on Model EVERCOOL SQUID magnetometer from *Quantum Design*.

3. Results and discussion

Fig. 1 shows the X-ray diffraction patterns of all the as-calcined samples – pure ZnO and ZnO:Ni with 2, 5, 7 and 10 at%. In the XRD pattern of undoped zinc oxide sample, all the observed peaks correspond to the wurtzite structure of ZnO. However, for ZN2 sample, a peak appearing at 2θ value of 37.26° corresponding to (1 1 1) plane of cubic NiO and for ZN5, ZN7 and ZN10 samples, an additional peak at 43.19°,corresponding to (2 0 0) planes of cubic NiO phase, is also observed. In ZN2, ZN5 and ZN7 samples, one peak of elemental Ni at 2θ value of 44.06° corresponding to (1 1 1) plane is also observed. The presence of elemental Ni shows that all Ni atoms do not go in the ZnO lattice and substitute Zn^{2+} ions. Some of the Ni atoms form clusters. In the diffractograms, the peaks due to NiO and Ni phases are indicated by symbols '*' and 'o' respectively.

The Rietveld refinement of the entire XRD data was carried out assuming wurtzite hexagonal structure. The crystallite size of various samples was also estimated using Debye–Scherrer formula after accounting for the instrumental broadening. Table 1 shows the refined lattice parameters (i.e., '*a*' and '*c*') and the crystallite

Table 1
Rietveld refined lattice parameters '*a*', '*c*' and the crystallite size of all the as-calcined samples.

Sample	Lattice parameters		Crystallite size (nm)
	'*a*' (Å)	'*c*' (Å)	
ZN1	3.251	5.213	41
ZN2	3.250	5.207	46
ZN5	3.248	5.203	51
ZN7	3.248	5.205	57
ZN10	3.248	5.201	56

size of all the as-calcined samples. It is seen that the lattice parameters '*a*', '*c*' decrease slightly as the concentration of Ni increases and finally becomes more or less constant. It may be noted that the ionic radii of the Ni^{2+} (i.e., 0.55 Å) is significantly smaller than Zn^{2+} (i.e., 0.60 Å) in the tetrahedral coordination. Thus, the observed decrease in lattice parameters could be satisfactorily ascribed to the substitution of Zn^{2+} by Ni^{2+}. The crystallite size of all as-calcined samples is found to slightly increase with increase in Ni concentration.

The DC-magnetization measurements of the undoped and doped zinc oxide samples were performed at room temperature. As expected, undoped zinc oxide was found to be diamagnetic. Fig. 2 shows the magnetization (M) versus field ($\mu_0 H$) plots of some of the as-calcined nanocrystalline ZnO:Ni samples having different Ni concentration. The observed M–$\mu_0 H$ behavior in these samples reveals that all the samples are purely ferromagnetic. It can be observed that the saturation magnetization first increases with increase in Ni concentration up to 7% and then decreases drastically for the sample with 10% Ni concentration. It may be recalled here that ZN10 sample does not exhibit any peak corresponding to the metallic nickel but exhibited a NiO peak of significant intensity. In the M–$\mu_0 H$ behavior, it is seen that the ZN10 sample exhibits lesser saturation magnetization (M_S), implying thereby that it has increased tendency of formation of NiO than for metallic nickel. Thus, the observed FM behavior could arise due to finite presence of Ni-clusters, as is evident from the XRD patterns of other calcined samples wherein Ni clusters were present (see Fig. 1). On the other hand, the observed FM behavior could be in part due to Ni substituted ZnO as well. We, therefore, decided to further sinter and investigate these ZnO:Ni samples at higher temperatures in presence of air with a aim to oxidize Ni completely.

An important thing to study/observe is how the different phases, i.e. wurzite ZnO, metallic nickel and cubic NiO, present in these

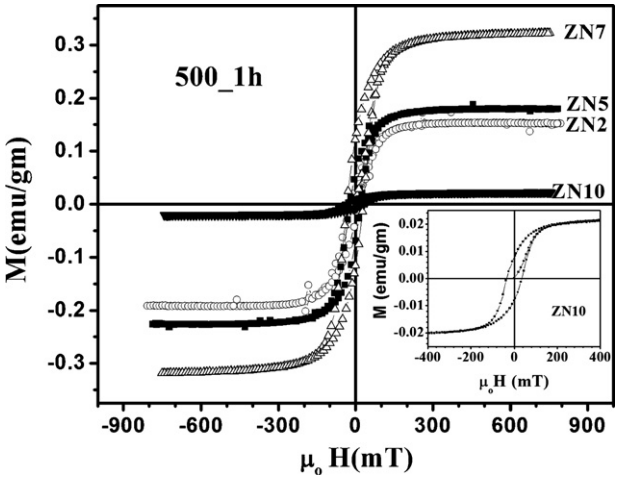

Fig. 2. M vs. $\mu_0 H$ data (recorded at 300 K) of the different as-calcined samples: ZN2, ZN5, ZN7 and ZN10. The calcination temperature and duration are indicated in the main panel. Inset shows the enlarged view of ZN10 sample.

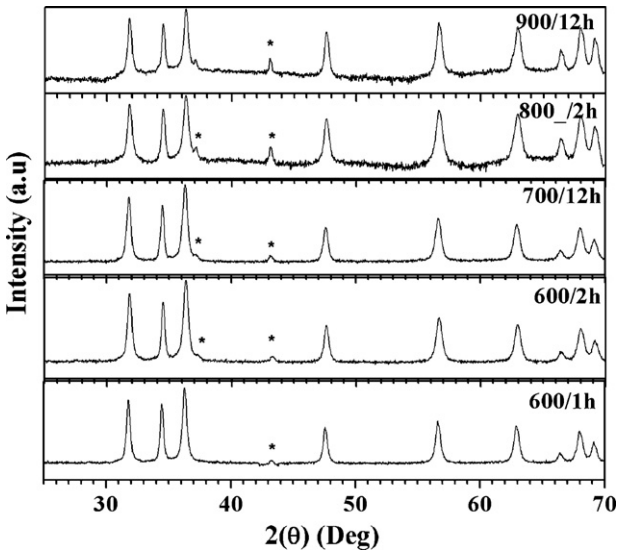

Fig. 3. Semilog XRD plots of ZN2 series sintered at different temperatures. The peaks arising due to NiO are indicated by symbol '*'.

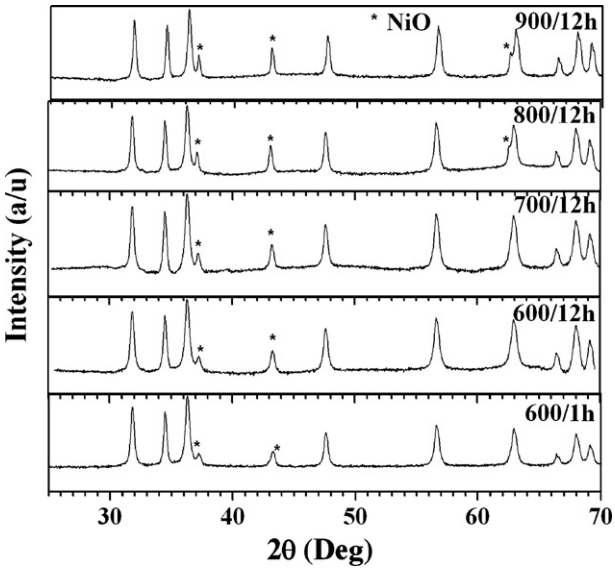

Fig. 5. Semilog XRD plots of ZN7 series sintered at different temperatures. The peaks arising due to NiO are indicated by symbol '*'.

samples evolve on sintering to higher and higher temperatures and how this affects the magnetic properties. Figs. 3–5 show the XRD plots of ZN2, ZN5 and ZN7 series samples, respectively, sintered at 600 °C for 1 h and then 12 h, followed by successive sintering at temperature of 700, 800 and 900 °C for 12 h duration at each temperature. It can be seen that in ZN2, ZN5 and ZN7 series samples, the peaks corresponding to NiO starts growing when the samples are sintered at 600 °C for even 1 h. It is also observed that the relative intensity of nickel oxide peaks in all the series samples increases as the samples are sequentially sintered at higher temperatures and it also increases with increase in Ni concentration. Also, the peak due to metallic Ni understandably disappears on sintering in air. It is to be noted that as the samples are sequentially sintered, the particle size increases. This is expected as the increase in sintering temperature provides energy required for growth of the grains once a desired phase is formed/nucleated. Since these samples that are sintered at high temperatures for long durations, we do not expect them to contain any amorphous phase.

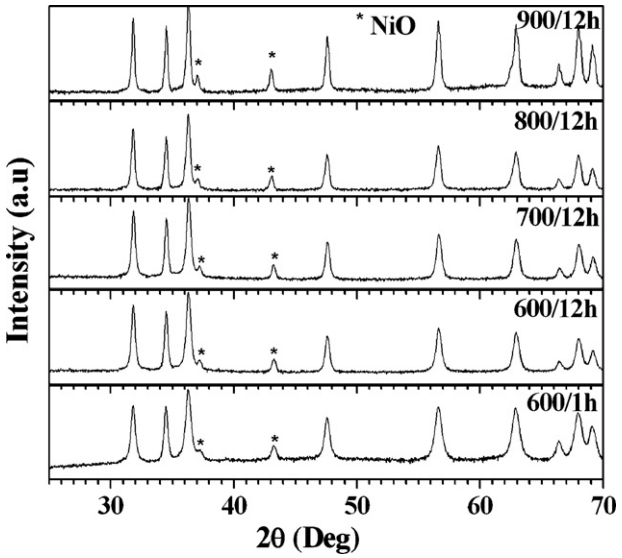

Fig. 4. Semilog XRD plots of ZN5 series sintered at different temperatures. The peaks arising due to NiO are indicated by symbol '*'.

Fig. 6 compares the M–$\mu_0 H$ plot of ZN2 series samples sintered at 500 and 600 °C for 1 h, respectively. It is observed that on sintering the ZN2 sample at 600 °C for 1 h, there is a large decrease in the saturation magnetization (about 7.5 times), but the sample still retains its complete ferromagnetic behavior. On sintering the ZN2 sample further at 600 °C for 12 h and then at 700, 800 and 900 °C for 12 h each, the samples exhibit a significantly different magnetic behavior (see Fig. 7(a) and (b)). In all these cases, absence of saturation in the magnetization and a distinct nonlinearity near the low field values is observed. The observed M–$\mu_0 H$ behavior (Fig. 7(a)) of this sample suggests that it contains at least two phases having different M–$\mu_0 H$ behavior, one whose contribution to M is linear in field with a net negative slope (this could be either due to diamagnetic (DM) or DM + paramagnetic (PM) or DM + antiferromagnetic (AF) or DM + PM + AF combinations) and the other whose M–$\mu_0 H$ behavior is like that of a FM phase. This implies that in ZN2 series sample, there is a significant diamagnetic contribution, which may be due to the dominance of unsubstituted parent ZnO. This is so because with sintering at higher temperatures, the magnitude of net negative slope (high field M-H region) is found to get reduced (see Fig. 7(a)). In our earlier studies [31] on chemically synthesized

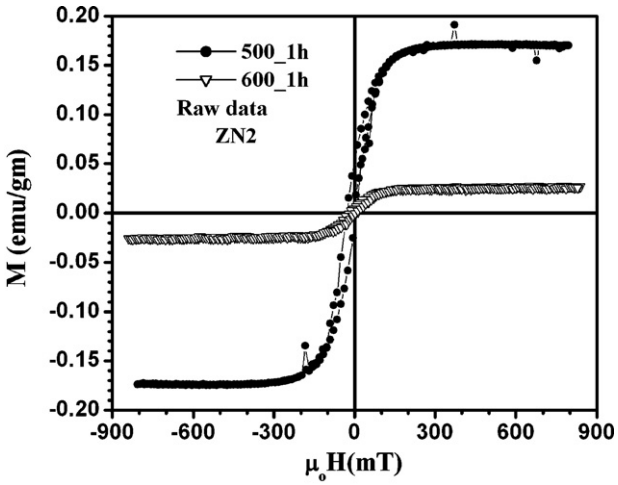

Fig. 6. Comparison of M–$\mu_0 H$ plots of ZN2 sample calcined at 500 and 600 °C for 1 h.

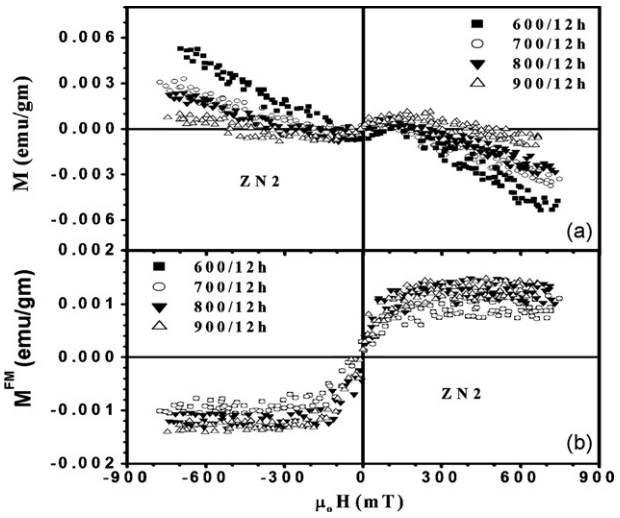

Fig. 7. (a) Raw M–$\mu_0 H$ data of ZN2 sample sintered at 600, 700, 800 and 900 °C and (b) extracted M–$\mu_0 H$ plots of the FM component present in ZN2 sample sintered at the indicated temperatures.

$Zn_{0.95}Co_{0.05}O$, we had concluded the some of the Co^{2+} ions that substitute Zn^{2+} ions give rise to ferromagnetic $Zn_{1-x}Co_xO$ (by forming bound magnetic polarons), while the uncorrelated Co^{2+} ions give rise to paramagnetic $Zn_{1-x}Co_xO$. The same can be true in the present case also, where some of uncorrelated Ni^{2+} ions that substitute Zn^{2+} ions can give rise to paramagnetic contribution. The magnetization due to the FM phase present in these samples has been extracted by using the slope of the linear part of the overall magnetization curves beyond the technical saturation, and is shown in Fig. 7(b) for the ZN2 series sample. It is observed that the total magnetization (M) and the saturation magnetization of the ferromagnetic fraction (M_S^{FM}) behave differently on sintering the sample to higher temperatures. The total magnetization first decreases significantly on sintering the sample to 600 °C for 1 and 12 h. However, on sintering to higher temperatures, the total magnetization tends to increase a little. On the other hand, the M_S^{FM} decreases significantly with the sequential sintering up to 600 °C for 12 h. Above 600 °C, the M_S^{FM} is more or less unaffected (see Fig. 7(b)). It is important to note that since magnetization values are small and near the detection sensitivity, nothing much can be concluded in this regard. However, if one compares the M_S^{FM} in the as-calcined and sintered samples, it is clear that high temperature sintering in air results in reduction of the saturation moment by nearly two orders of magnitude. Together with the XRD findings, this suggests that nickel clusters are oxidized on sintering to 600 °C, which makes the sample robust, since M_S^{FM} becomes independent of subsequent sintering. The increase in the total magnetization on subsequent sintering could be understood due to the formation of more and more antiferromagnetic NiO on sintering at higher temperatures.

Fig. 8(a) shows the raw M–$\mu_0 H$ plot of ZN5 series sample. The observed M–$\mu_0 H$ behavior of this sample after sintering at 600 °C/1 h, and then 600 °C/12 h is found to be the mixture of overall diamagnetic/paramagnetic ZnO:Ni and ferromagnetic phases. On further sintering at 700 °C/12 h, 800 °C/12 h and 900 °C/12 h, the M–H behavior of the antiferromagnetic NiO fraction dominates over the diamagnetic fraction of unsubstitutued ZnO and the sample is then found to be the mixture of ferromagnetic and other phases with linear M–$\mu_0 H$ behavior with a net positive susceptibility. This conjecture is supported by the XRD investigations where the amount of nickel oxide is found to increase with sequential sintering. The saturation magnetization of the FM fraction (Fig. 8(b)) decreases significantly on sintering at 600 °C for 12 h and then becomes constant on further sintering at higher temperatures, similar to the case of ZN2 sample. Fig. 9(a) shows the M–$\mu_0 H$ plot of ZN7 sample. The sample is found to be a mixture of FM and PM/AF phases. The important point to be noted here is that even the sample annealed at 600 °C consists of a mixture of FM and AF phases in sharp contrast to the case when Ni concentration was less than 7%. In view of the supporting XRD results, here, again the high field linear M–$\mu_0 H$ behavior is attributed to the AF NiO phase, whose fraction increases as the sample is sintered at higher temperatures. Fig. 9(b) shows the M–$\mu_0 H$ behavior of the extracted FM fraction present in the ZN7 sample. The magnetization results of ZN10 sample, not shown here for conciseness, are similar to that of ZN7 samples.

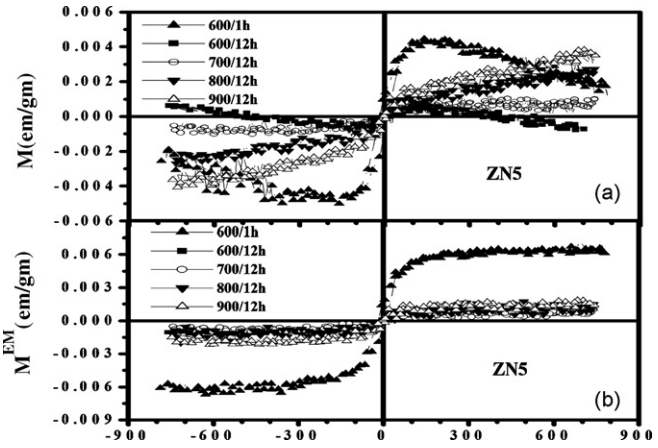

Fig. 8. (a) Raw M–$\mu_0 H$ data of ZN5 sample sintered at 600, 700, 800 and 900 °C and (b) extracted M–$\mu_0 H$ plots of the FM component present in ZN5 sample sintered at the indicated temperatures.

If we compare the total magnetization values (i.e., emu/g of the sample) among the different samples, say at 500 mT, it is observed that for the samples calcined at 500 °C/1 h, the ZN7 has the highest saturation magnetization value (Fig. 2). When the samples are sintered at a higher temperature of 600 °C/1 h, this value is highest for ZN2 sample (compare Figs. 6 and 9(a)). On further sintering to 600 °C/12 h, the samples exhibit a very different behavior. At this stage, the ZN2 and ZN5 samples exhibit a FM + DM (there may be some PM component also) behavior whereas ZN7 and ZN10 exhibit a FM + PM/AF behavior. This is because of the presence of more NiO in these samples, which tends to mask the behavior of DM par-

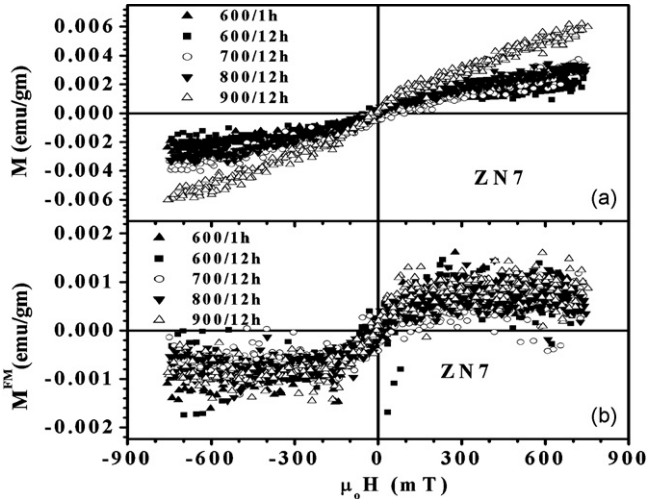

Fig. 9. Raw M–$\mu_0 H$ data of ZN7 sample sintered at 600, 700, 800 and 900 °C and (b) extracted M–$\mu_0 H$ plots of the FM component present in ZN7 sample sintered at the indicated temperatures.

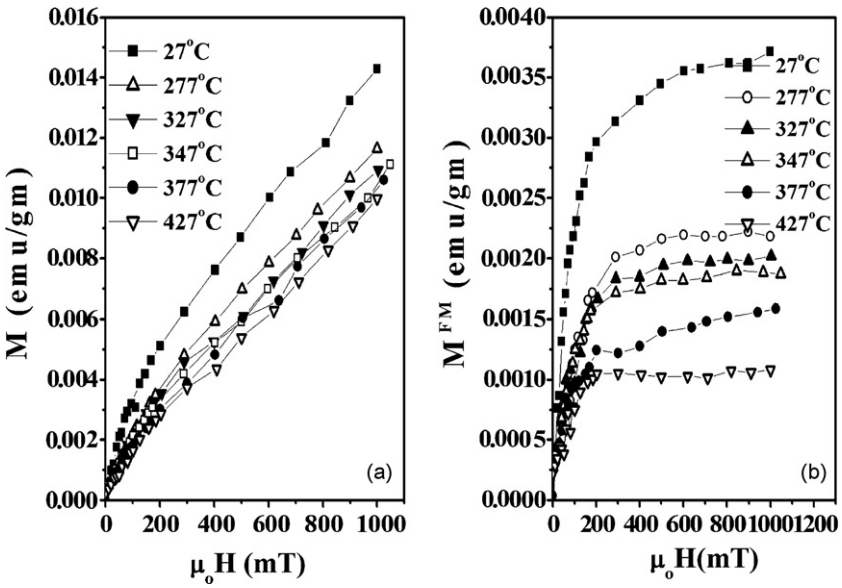

Fig. 10. (a) Raw M–$\mu_0 H$ and (b) extracted M–$\mu_0 H$ plots of the ferromagnetic fraction present in ZN10 sample finally sintered at 900 °C/12 h (data recorded using SQUID at measurement temperatures of 27, 277, 327, 347, 377 and 427 °C (300, 550, 600, 620, 650 and 700 K).

ent/unsubstituted ZnO, and/or PM fraction due to the uncorrelated or noninteracting Ni^{2+} ions substituted for Zn^{+2} in the sample. However, on sintering the ZN5 sample to 700 °C/12 h, the contribution of the diamagnetic ZnO becomes equal to the growing AF/PM contribution and both cancel each other giving an impression that the ZN5 sample is fully ferromagnetic at 700 °C/12 h. At still higher temperatures, the ZN5 sample exhibits FM + AF/PM behavior, whereas in ZN2 sample some amount of unreacted diamagnetic ZnO is always present. It seems that at higher temperatures, the solubility limit of Ni in ZnO is even less than 2%. The AF component increases with increase in sintering due to formation of more and more NiO at higher temperatures. The MFM_S of all the samples (sintered at 900 °C/12 h) tend to be almost equal, as if it is governed by the solubility limit. This is similar to that observed in our chemically synthesized ZnO:Co samples [32]. Thus, in the present case, the samples calcined at lower temperatures (upto 600 °C/1 h) consist of unreacted diamagnetic ZnO, ferromagnetic metallic Ni clusters, small amount of antiferromagnetic NiO, a ferromagnetic $Zn_{1-x}Ni_xO$. It is also possible that some Ni going in ZnO lattice forms paramagnetic $Zn_{1-x}Ni_xO$, as is observed in our $Zn_{1-x}Co_xO$ nanocrystalline samples as well as thin films [33]. As we increase the sintering temperature, the metallic Ni oxidizes and the fraction of the rest of components also changes. But, based on the M–$\mu_0 H$ data acquired, it is not possible to calculate the fraction of individual components. It is important to note that the at% doping level used as the start of the sample preparation (as calcined samples) does not remains as such after sintering at 900 °C, it is because some of the nickel forms clusters of metallic nickel (at lower synthesis temperatures) and nickel oxide. The amount of these two changes on sintering as observed from the XRD data. It is to be noted that the other complexes (for example carbon) used for synthesis of these samples, are not expected to effect the results, as the pure ZnO synthesized by the same method is found to be diamagnetic.

It is not possible to determine the amount of nickel that forms (a) NiO and (b) paramagnetic $Zn_{1-x}Ni_x$ O from the global measurement techniques (XRD and VSM measurements) employed in this paper, hence the saturation value of the magnetization cannot be exactly determined. However, if we suppose all the Ni^{2+} substitutes Zn^{2+} in the ZnO lattice, the observed saturation magnetization per doped Ni ion in case of ZN2 is: 0.123 μ_B at 500/1 h, 0.028 μ_B at 600/1 h and 7.27×10^{-4} μ_B at higher temperatures. For ZN5 this value is 0.052 μ_B at 500/1 h, 0.0017 μ_B at 600/1 h and above. For ZN7, it is 0.066 μ_B at 500/1 h and 1.5×10^{-4} μ_B at higher temperature. But these values are very much underestimated as the fraction of nickel that might give rise to the observed saturation magnetization of FM fraction could be very much less than that used for calculation of the above values.

From the M–$\mu_0 H$ investigations, we also note that the saturation magnetization of the FM component present in the sample sintered at high temperatures always remained between $0.5–1.5 \times 10^{-3}$ emu/g, irrespective of large variation of Ni concentration (1–10%). This together with the XRD observations, namely (a) increase of peak intensity due to NiO phase within same Ni-concentration series with the sintering temperatures, and (b) relatively less change of lattice parameter with the Ni incorporation in ZnO, indicate that solid solubility of Ni is limited to significantly less than 10% in ZnO. In literature, it has also been reported that the solubility limit of Ni in nanocrystalline ZnO powder prepared by chemical methods is quiet low as compared to other transition metals like Co or Mn [34]. It is only upto 3 at% of Ni in ZnO, when the samples are prepared at a temperature of 300 °C and it decreases further as the synthesis temperature is increased.

In order to have a clue about the origin of RTFM, the high temperature isothermal M–$\mu_0 H$ measurements were carried out on ZN10 sample sintered upto 900 °C. Fig. 10(a) shows the isothermal virgin M–$\mu_0 H$ plots recorded at different temperatures ranging from 27 to 427 °C (300–700 K). It is observed that as expected, the net magnetization decreases with increase in temperature. But the nonlinearity in the data exists even at 427 °C (700 K), which clearly indicates that the observed ferromagnetism is not due to nickel clusters. The Curie temperature of metallic nickel is 358 °C (i.e., 631 K). Fig. 10(b) shows the M–$\mu_0 H$ behavior of the ferromagnetic fraction present in the ZN10 sample.

The observed temperature dependence of the magnetization behavior can also be used to see if the present samples exhibit any trace of possible superparamagnetic behavior. It is known that two aspects of superparamagnetic behavior are always true, i.e. (a) the M–$\mu_0 H$ curves plotted at different T superimpose, when M/M_S is plotted as function of H/T, and (b) there is no hysteresis in the M–$\mu_0 H$ behavior [35]. The M/M_S versus $\mu_0 H/T$ curves derived from the isothermal M–$\mu_0 H$ data recorded using SQUID magnetometer at 27, 347 and 427 °C (300, 620 and 700 K) of the FM fraction present

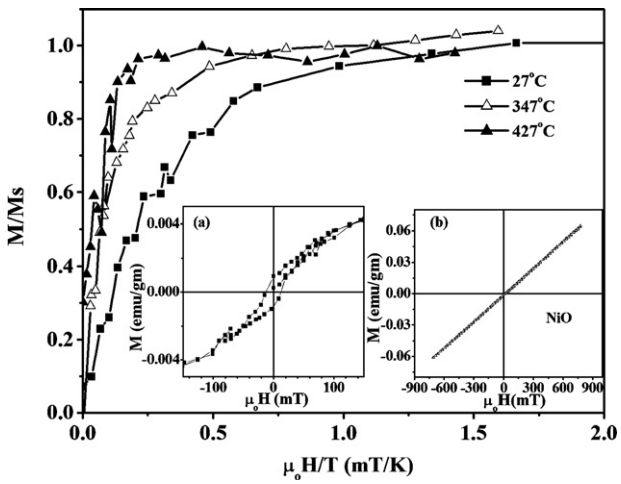

Fig. 11. The M/M_S vs. $\mu_0 H/T$ plots of ferromagnetic component present in ZN10 sample sintered at 900 °C/12 h (using data recorded T = 300, 620 and 700 K). Inset (a) shows the enlarged view of the full M–$\mu_0 H$ loop near origin (data recorded at T = 300 K). Inset (b) shows the M–$\mu_0 H$ plot for the NiO sample recorded at 300 K using VSM.

in 900 °C/12 h annealed ZN10 sample are plotted in the Fig. 11. Both, the absence of superimposition of the M/M_S versus $\mu_0 H/T$ plots and the hysteretic M–$\mu_0 H$ plots (coercivity ~12.5 mT as inferred from the inset (a) of Fig. 11), thus, undoubtedly proves that the observed saturation of the moment is not due to superparamagnetic behavior.

We also rule out that the presence of observed RTFM is due to nanoparticles of nickel, as the Curie temperature is known to decrease with decrease in size of the ferromagnetic nanoparticles (<10 nm) [36,37]. If it had been the case, T_C would be lower than 631 K. In some cases, it has also been reported that small NiO particles exhibit superparamagnetic [38] or spin glass [39] behavior. This occurs when the particle size is very small [38] and/or the samples are synthesized at low temperatures of 120 or 350 °C [39]. In the present case, the samples are annealed at higher temperatures upto 900 °C, so we do not expect the present samples to show such behavior. The M–$\mu_0 H$ data of the pure NiO sample prepared by same chemical route and sintered at 900 °C is shown in inset of Fig. 11.

In the as-calcined nickel incorporated ZnO nanocrystalline powder samples, the ferromagnetism is due to the formation of the secondary phases of Ni clusters (as observed from the XRD data). But as the samples are sequentially sintered to higher temperatures, Ni peaks are not found in XRD data, instead NiO is predominanently detected. It may be noted that the original state of the sample cannot be recovered by annealing the compounds. Furthermore, all the samples exhibit RTFM behavior. It suggests that in as-calcined samples, this RTFM is predominantly due to the Ni clusters. However, in all the sintered samples, this ferromagnetism originates definitely due in part to the partial substitution of Ni^{2+} ions at Zn-sites. The observance of FM behavior at temperatures (Fig. 10) higher than T_C of Ni supports this conclusion. The high field linear M–$\mu_0 H$ in these samples is due to antiferromagnetic NiO formed as a result of oxidation of the Ni-clusters due to prolonged sintering in air, as is evidenced by XRD investigations.

These nickel incorporated ZnO powder samples exhibit high resistivity. It suggests that the free carrier mediated Rudermann–Kittel–Kasuya–Yosida (RKKY) interaction may not be responsible for the FM ordering in the present case. The insulating nature of these samples rather hints that the bound magnetic polaron (BMP) model [40] proposed for magnetic ordering in insulating systems could possibly account for the observed RTFM in the present case. In this model, the ferromagnetism may arise due to the interaction of bound magnetic polarons. A bound magnetic polaron (BMP), consists of a localized hole/electron and a large number of magnetic impurities around the localized charge. Though, the direct exchange between localized carriers is antiferromagnetic, the interaction between BMP may be FM like at large enough concentration of magnetic impurities. This model is applicable when the carrier concentration is much less than the concentration of magnetic impurities. Thus, the overlapping polarons (or the so called BMP) might correlate, and give rise to FM contribution as is experimentally observed. However, at the same time, the isolated polarons can contribute to the PM fraction, i.e. those noninteracting nickel ions, not taking part in the formation of BMPs, account for the overall PM contribution of the $Zn_{1-x}Ni_xO$ samples. It is to be emphasized here that the RTFM in Ni-incorporated ZnO is relatively weak compared to Co incorporated ZnO [4,25,26]. It requires more experimental investigations to confirm the applicability of the polaron model in the present ZnO:Ni systems. Alternatively, the observed FM in the present case could also be defect mediated as suggested by Coey et al. [41]. In the present case, the samples that are sintered at high temperatures for long durations, so we do not expect the sample to contain any amorphous phase that could give rise to the observed ferromagnetism. However, we do not rule out any such possibility or other alternate explanation of the origin of FM in this system.

4. Conclusions

The ZnO:Ni samples with Ni concentration upto 10% are synthesized by chemical method using acetates and poly vinyl pyrolidane as precursors. The effect of sintering on the magnetization behavior of ZnO:Ni was studied in detail. The samples calcined at 500 °C/1 h are ferromagnetic and this ferromagnetism arises from the metallic nickel as evidenced from the XRD studies. On sintering the samples to higher temperature, metallic nickel oxidizes to nickel oxide with the result that the saturation magnetization of the samples decreases. It is observed that on sintering the samples at further higher temperatures, the relative intensity of the NiO peak increases. It is clearly demonstrated that on sintering these samples in air upto 900 °C/12 h, the samples are a mixture of FM, AF, PM and/or DM fractions, depending upon the temperature dependent solubility limit of Ni in ZnO. The observed RTFM, though weak, evidenced in ZnO:Ni samples sintered at 900 °C/12 h persists even at 700 K (higher than the Curie temperature of metallic nickel), appears to be an intrinsic effect.

References

[1] T. Dietl, H. Ohno, F. Matsukur, J. Cibert, D. Ferrad, Science 287 (2000) 1019.
[2] K. Sato, H.K. Yoshida, Jpn. J. Appl. Phys. Part 2 39 (2000) L555.
[3] C. Song, K.W. Geng, F. Zheng, X.B. Wang, Y.X. Shen, F. Pan, Y.N. Xie, T. Liu, H.T. Zhou, Z. Fan, Phys. Rev. B 73 (2006) 024405.
[4] K.P. Bhatti, S. Chaudhary, D.K. Pandya, S.C. Kashyap, J. Appl. Phys. 101 (2007) 033919.
[5] D.A. Schwartz, K.R. Kittilstved, D.R. Gamelin, Appl. Phys. Lett. 85 (2004) 1395.
[6] T. Li, H. Qiu, P. Wu, M. Wang, R. Ma, Thin Solid Films 515 (2007) 3905.
[7] E. Liu, P. Xiao, J.S. Chen, B.C. Lim, L. Li, Curr. Appl. Phys. (2007), doi:10.1016/j.cap.2007.10.025.
[8] X. Liu, F. Lin, L. Sun, W. Cheng, X. Ma, W. Shi, Appl. Phys. Lett. 88 (2006) 062508.
[9] W. Yu, L.H. Yang, X.Y. Teng, J.C. Zhang, Z.C. Zhang, L. Zhang, G.S. Fu, J. Appl. Phys. 103 (2008) 093901.
[10] J.C. Pivin, G. Socol, I. Mihailescu, P. Berthet, F. Singh, M.K. Patel, L. Vincent, Thin Solid Films 517 (2008) 916.
[11] K.T. Kim, G.H. Kim, J.C. Woo, C.I. Kim, Surf. Coat. Technol. 202 (2008) 5650.
[12] Z.L. Lu, W. Miao, W.Q. Zou, M.X. Xu, F.M. Zhang, J. Alloys Compd. 494 (2010) 392.
[13] B. Pandey, S. Ghosh, P. Srivastava, D.K. Avasthi, D. Kabiraj, J.C. Pivin, J. Magn. Magn. Mater. 320 (2006) 3347.
[14] Z. Yin, N. Chen, F. Yang, S. Song, C. Chai, J. Zhong, H. Qian, K. Ibrahim, Solid State Commun. 135 (2005) 430.
[15] J.B. Cui, U.J. Gibson, Appl. Phys. Lett. 87 (2005) 133108.

[16] P.V. Radovanovic, D.R. Gamelin, Phys. Rev. Lett. 91 (2003) 157202.
[17] Z.X. Cheng, X.L. Wang, S.X. Dou, K. Ozawa, H. Kimura, P. Munroe, J. Phys. D: Appl. Phys. 40 (2007) 6518.
[18] C.J. Cong, J.H. Hong, Q.Y. Liu, L. Liao, K.L. Zhang, Solid State Commun. 138 (2006) 511.
[19] H. Wang, Y. Chen, H.B. Wang, C. Zhang, F.J. Yang, J.X. Duan, C.P. Yang, M. Xu, M.J. Zhou, Q. Li, Appl. Phys. Lett. 90 (2007) 052505.
[20] C. Cheng, G. Xu, H. Zhang, Y. Luo, Mater. Lett. 62 (2008) 1617.
[21] M.E. Hilo, A.A. Dakhel, A.Y.A. Mohamed, J. Magn. Magn. Mater. 321 (2009) 2279.
[22] S. Zhou, K. Potzger, K. Kuepper, J. Grenzer, M. Helm, J. Fassbender, E. Arenholz, J.D. Denlinger, J. Appl. Phys. 103 (2008) 043901.
[23] T. Liu-Niu Tong, H. Cheng, J. Han, Lian Hu, Y. Xian-Mei He, C.M. Tong, Schneider, J. Appl. Phys. 108 (2010) 023906.
[24] D.-L. Houa, R.-B. Zhaoa, Y.-Y. Weia, C.-M. Zhena, C.-F. Pana, G.-D. Tanga, Curr. Appl. Phys. 10 (2010) 124.
[25] E.S. Kumar, S. Venkatesh, M.S. Ramachandra Rao, Appl. Phys. Lett. 96 (2010) 232504.
[26] Z. Yu, S. Ge, Y. Zuo, G. Wang, F. Zhang, Appl. Surf. Sci. 256 (2010) 5813.
[27] M/ Yu, H. Qiu, X. Chen, H. Liu, Mater. Chem. Phys. 120 (2010) 571.
[28] X. Mao, W. Zhong, Youwei Du, J. Magn. Magn. Mater. 320 (2008) 1102.
[29] S. Zhou, K. Potzger, G. Zhang, F. Eichhorn, W. Skorupa, M. Helm, J. Fassbender, J. Appl. Phys. 100 (2006) 114304.
[30] J. Alaria, M. Venkatesan, J.M.D. Coey, J. Appl. Phys. 103 (2008) 07D123.
[31] K.P. Bhatti, S. Kundu, S. Chaudhary, D.K. Pandya, S.C. Kashyap, J. Phys. D: Appl. Phys. 39 (2006) 4909.
[32] K.P. Bhatti, S. Chaudhary, D.K. Pandya, S.C. Kashyap, J. Appl. Phys. 101 (2007) 033902.
[33] S. Chaudhary, K.P. Bhatti, D.K. Pandya, S.C. Kashyap, A.K. Nigam, J. Magn. Magn. Mater. 321 (2009) 966.
[34] S.K. Mandal, A.K. Das, T.K. Nath, D. Karmakar, Appl. Phys. Lett. 89 (2006) 144105.
[35] B.D. Cullity, Introduction to Magnetic Materials, Addison-Wesley, Reading, MA, 1972, p. 114, Fig. 3.13.
[36] H.M. Lu, P.Y. Li, Y.N. Huang, X.K. Meng, X.Y. Zhang, Q. Liu, J. Appl. Phys. 105 (2009) 023516.
[37] H. Amekura, Y. Fudamoto, Y. Takeda, N. Kishimoto, Phys. Rev. B 71 (2009) 172404.
[38] J.N. Herak, B. Rakvin, Phys. Lett. A 53 (1974) 307.
[39] S.D. Tiwari, K.P. Rajeev, Thin Solid Films 505 (2006) 113.
[40] A. Kaminski, S.D. Sarma, Phys. Rev. Lett. 88 (2002) 247202.
[41] J.M.D. Coey, M. Venkateshan, C.B. Fitzgerald, Nat. Mater. 4 (2005) 173.